Draft version March 3, 2013
Preprint typeset using LaTeX style emulateapj v. 04/20/08

arXiv:1205.0083v1 [astro-ph.CO] 1 May 2012

THE EMISSION-LINE SPECTRA OF MAJOR MERGERS: EVIDENCE FOR SHOCKED OUTFLOWS [1]

Kurt T. Soto[1], C. L. Martin[1], M. K. M. Prescott[1], L. Armus[2]
[1] Physics Department, University of California, Santa Barbara, CA 93106-9530
[2] Spitzer Science Center, California Institute of Technology, Pasadena, CA.

Draft version March 3, 2013

ABSTRACT

Using a spectral decomposition technique (Soto & Martin 2012, hereafter Paper I), we investigate the physical origin of the high-velocity emission line gas in a sample of 39 gas-rich, ultraluminous infrared galaxy (ULIRG) mergers. Regions with shock-like excitation were identified in two kinematically distinct regimes, characterized by broad ($\sigma > 150$ km s^{-1}) and narrow linewidths. Here we investigate the physical origin of the high-velocity (broad) emission with shock-like line ratios. Considering the large amount of extinction in these galaxies, the blueshift of the broad emission suggests an origin on the near side of the galaxy and therefore an interpretation as a galactic outflow. The large spatial extent of the broad, shocked emission component is generally inconsistent with an origin in the narrow-line region of a AGN, so we conclude that energy and momentum supplied by the starburst drives these outflows. The new data are used to examine the fraction of the supernova energy radiated by shocks and the mass loss rate in the warm-ionized phase of the wind. We show that the shocks produced by galactic outflows can be recognized in moderately high-resolution, integrated spectra of these nearby, ultraluminous starbursts. The spectral fitting technique introduced in Paper I may therefore be used to improve the accuracy of the physical properties measured for high-redshift galaxies from their (observed frame) infrared spectra.

Subject headings: galaxies: starburst — galaxies: evolution — galaxies: active — galaxies: formation

1. INTRODUCTION

Ultraluminous infrared galaxies (ULIRGs) are some of the most powerful galaxies in the local universe, with $\log(L_{IR}/L_\odot) > 12$. Many ULIRGs exhibit disturbed morphology which indicates that they are major mergers (Borne et al. 1999). Tidal interactions in major mergers are believed to drive gas inflow that fuels both the starbursts and the active galactic nuclei (AGN) in ULIRGs (Toomre & Toomre 1972; Sanders et al. 1986; Springel et al. 2005; Hopkins et al. 2008).

Models of major mergers also predict an early phase of supernova feedback followed by the emergence of an AGN (Springel et al. 2005; Hopkins et al. 2005; Hopkins 2012). Starburst-driven outflows are found in $75 - 80\%$ of ULIRGs (Rupke et al. 2002; Martin 2005). Interstellar absorption lines in their spectra are blueshifted a few hundred km s^{-1} relative to the systemic velocity set by the molecular gas and stars (Armus et al. 1990; Heckman et al. 1990; Martin 2005, 2006; Rupke et al. 2005a,b,c; Rupke & Veilleux 2005). AGN-driven outflows, in contrast, have only been found in the small subset of ULIRGs with Seyfert 1 nuclei (Rupke et al. 2005a), possibly indicating that these systems are no longer classified as ULIRGs by the time AGN drive the outflows. Because the measured stellar velocity dispersions of ULIRGs typically exceed the stellar rotation speed and the surface brightness profiles fit $r^{1/4}$ laws (Genzel et al. 2001), as in elliptical rather than spiral galaxies, removal of the gas – whether by star formation, black-hole fueling, or outflow – provides the last step in transforming ULIRGs into field elliptical galaxies (Dasyra et al. 2006).

The high SFRs common among $z \sim 2 - 3$ galaxies are thought to be fueled by steady gas accretion instead of mergers (Daddi et al. 2007; Shapiro et al. 2008; Noguchi 1999), but mergers may play a pivotal role in the formation of galactic spheroids even at these redshifts (Hopkins et al. 2011). Regardless of how these galaxies get their gas, comparable star formation rates are only found among ULIRGs and the Lyman-Break Analogs (Overzier et al. 2008, 2009b,a, 2011; Heckman et al. 2011) in the local universe, so these environments provide the best local laboratories for studying the feedback processes that shape the evolution of high-redshift galaxies.

Given the importance of incorporating feedback from massive stars and AGN into galaxy formation simulations, simultaneously mapping out the excitation *and* gas kinematics in these extreme, local environments is of broad interest (Heckman et al. 1987; Armus et al. 1990; Heckman et al. 1990; Murray et al. 2005; Veilleux et al. 2009). The emission-line spectrum of shocked regions, for example, is easily distinguished from the spectrum of gas photoionized by massive stars but quite similar to the spectrum of gas photoionized by an AGN. Because the size of the narrow-line region (NLR) powered by AGN is limited by the AGN luminosity (Bennert et al. 2006a,b; Greene et al. 2011), one strategy for breaking this degneneracy between excitation mechanisms is to resolve the location of the gas emitting the *shock-like* spectrum (Monreal-Ibero et al. 2006; Rich et al. 2011; Gonçalves et al. 2010, , Paper I). Large velocity dispersions provide another way to identify regions with strong feedback from star formation and active nuclei, gravitational instability, and/or streams of recently accreted material (Genzel et al. 2011; Law et al. 2009; Schreiber et al. 2006) and the Doppler shifts of broad emission-lines can be used to distinguish shocks generated by galactic winds and infall from either cold streams or tidally stripped gas.

---

[1] The data presented herein were obtained at the W.M. Keck Observatory, which is operated as a scientific partnership among the California Institute of Technology, the University of California and the National Aeronautics and Space Administration. The Observatory was made possible by the generous financial support of the W.M. Keck Foundation.

To provide a more comprehensive examination of the location and speeds of shocks in ULIRGs, we mapped the emission-line ratios across 39 local ($z = 0.043 - 0.152$) ULIRGs in velocity *and* one spatial direction. These longslit spectra obtained with the Keck Echellette Spectrograph and Imager (ESI) lack the complete spatial coverage of integral field spectra (IFU) but offer more sensitivity and broader spectral coverage than IFU observations. In Paper I, we identified the regions with shock-like line ratios. Following a brief summary of the sample and observations in Section 2 of this paper, the velocity dispersion and Doppler shift of the shocked regions are presented in Section 3, where we argue that outflows are the primary origin of those shocked regions with broad ($\sigma > 150$ km s^{-1}) emission lines. In Section 4, we discuss the origin of the outflows and estimate the outflow properties. Finally, we discuss the impact of shocked gas on the integrated spectrum in Sect. 5.1.

2. OBSERVATIONS AND REDUCTIONS

This study examines the measurements presented in Paper I of 39 ULIRGs at various stages of merging chosen from from the IRAS 2 Jy survey (Murphy et al. 1996). These local galaxies span $z = 0.043 - 0.163$, allowing spatially resolved optical spectroscopy with the Keck ESI $1'' \times 20''$ long slit. The data were reduced as described in Martin (2005). Emission lines in the galaxies have $\sim$70 km s^{-1} spectral resolution and $\approx 0.8''$ spatial resolution limited by the atmospheric seeing. The median spatial resolution is 1.5 kpc, with a range of 0.7 to 2.1 kpc depending on redshift.

3. RESULTS

In Paper 1, we decomposed the emission line profiles into multiple Gaussian components. An example of this decomposition is shown in Figure 1. Because we jointly fit several transitions, we measured diagnostic line ratios for each velocity component. Using kpc-scale apertures, we mapped the Doppler shift, velocity width, and line fluxes across the ULIRGs. The results, provided in Table 3 of Paper 1, were used to classify the excitation mechanism of each component as HII-like or shock-like. Here, we explore the relationship between the gas kinematics and the excitation mechanism.

For each velocity component at a given spatial location, we classified the excitation mechanism as HII-like or shock-like using diagnostic ratios of line fluxes (Kewley et al. 2006). The [OI]/Ha ratio plays a major role in this categorization due to its high sensitivity to shocks. In cases where [OI]/Ha is obscured by telluric absorption, we rely on [SII]/Ha and [NII]/Ha to make this distinction. If the errors in the flux ratio cross the maximum star formation line, then the excitation mechanism is designated "unclear". We note that our "unclear" category differs from the composite classification of Kewley et al. (2006), defined by line ratios between the empirically defined maximum star formation limit and the maximum star formation. We further describe these categories and the fitting method in Paper I.

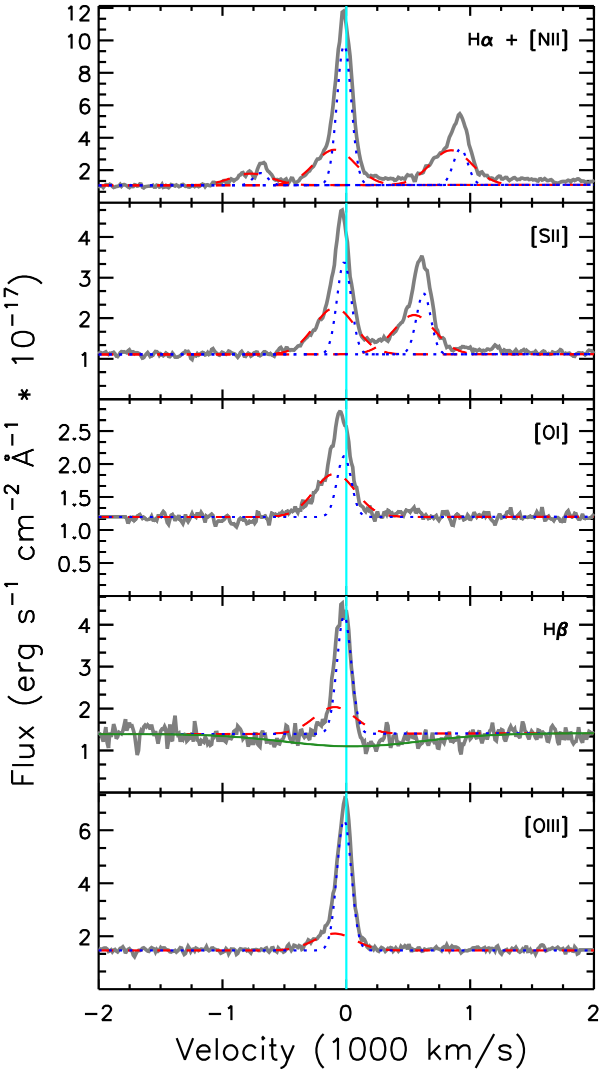

FIG. 1.— Example of emission-line fit from paper I; the line profiles of the different transtions were fit with common kinematic components of varying flux. This figure demonstrates the clear variations in the line profiles for each transition, i.e. the blueshifted wing on Hα, the nearly triangular line profile of [N II]λ6583, and the very low intensity blue wing on [O III]λ5007. Using this fitting method, we are able to deconstruct the line profile and examine the excitation mechanism for all of the spectral components that show the same kinematics.

Figure 2 shows a histogram of the velocity dispersions of the components from all apertures across all galaxies divided by excitation class. Spectral components classified as "HII-like" are narrow in linewidth, having $\sigma_v \leq 150$ km s^{-1}. The components identified as "shock-like", however, present a high-velocity tail at $\sigma_v > 150$ km s^{-1}. Clearly the broad components are preferentially shock excited.

We show the Doppler shift of all the components in Figure 3. The narrow, shock-like components (and the HII components) are detected over distances of $15 - 30$ kpc along the slit. The velocity offsets relative to the galaxy redshift are positive in one direction and negative to the opposite side of the nucleus. Figure 5 of Paper 1 demon-

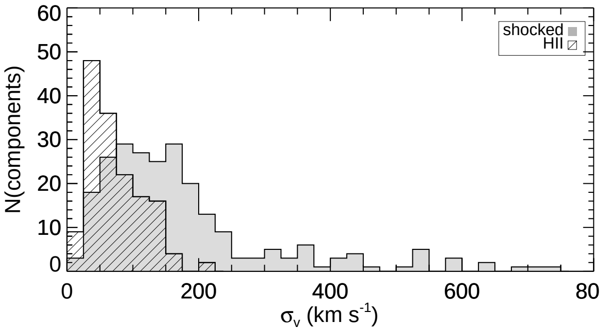

FIG. 2.— In the above histograms we present the distributions of line width for components identified as "shock-like" and those identified as "HII". Nearly all components with "HII" line ratios have $\sigma_v < 150$ km s^{-1}. The distribution of components identified as "shock-like" has a tail out to large line widths. (Of the 430 components measured, 34 copomnents are not shown here because the measurement uncertainties did not place them uniquely in one of these two excitation classes.)

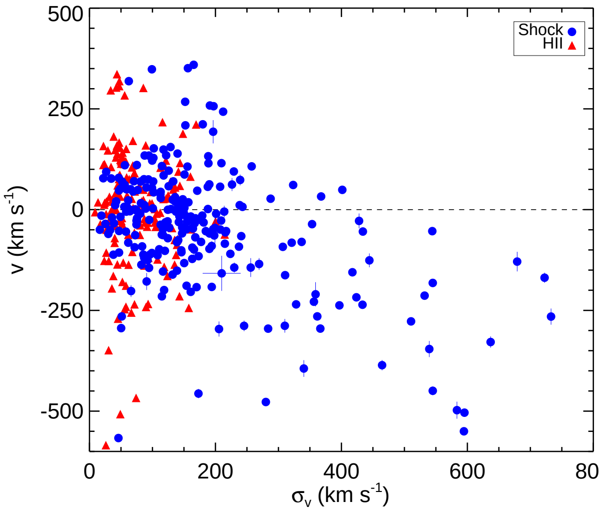

FIG. 3.— We find that the components identified as shock-like with $\sigma_v < 150$ km s^{-1} have a similar distribution in Doppler shift as the HII components. The shock-like components with $\sigma_v > 150$ km s^{-1}, however, present significant blueshifts.

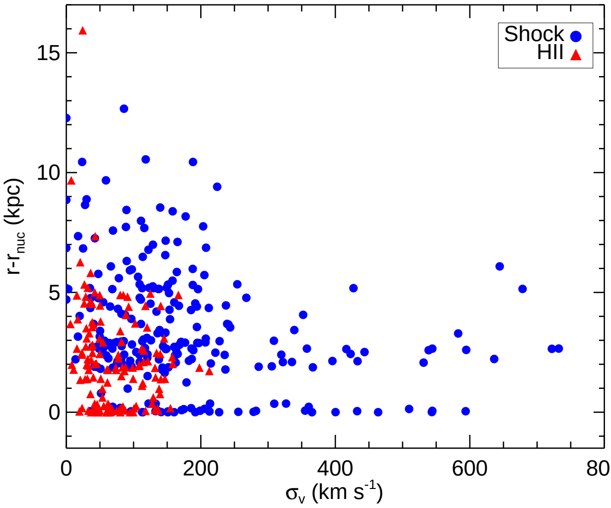

FIG. 4.— HII and shock-like components with $\sigma_v < 150$ km s^{-1} extend to regions 15 kpc away from their associated nuclei. Components with $\sigma_v > 150$ km s^{-1}, however, remain within 5 kpc of the nucleus. The gap between the points at $r = r_{nuc}$ and rest of the distribution reflects the spatial resolution of the spectroscopy.

strates that the position-velocity diagrams for these narrow, shock-like components are typically consistent with the projection of a galactic rotation curve, suggesting the process producing narrow, shock-like emission components is associated with a gas disk.

The broader components with $\sigma_v > 150$ km s^{-1}, however, do not show similar rotation gradients, suggesting that a different physical mechanism is involved in producing the broad emission. Figure 3 shows that the broad, shocked components are nearly always blueshifted in stark constrast to the narrow components. The blueshifts of the broad, shocked components reach a maximum of 500 km s^{-1}.

Because the ULIRGs are very dusty galaxies, their nuclei are not transparent at optical wavelengths. Hence, the emission-line radiation that we detect at the center of a ULIRG must be emitted on the near side of the dusty, gaseous disk. We therefore conclude that the blueshifted emission comes from outflowing gas on the near-side of the galaxy rather than infall on the far side. The broad emission in adjacent apertures maintain similar kinematics, which allows us to assume that these regions have similar dust obscuration. In support of this outflow interpretation, we note that the broad, shocked emission spans a velocity range quite similar to that of the blueshifted Na I absorption troughs previously identified in these spectra (Martin 2005, 2006).

Using the spatial information along the slit, we traced the extent of each spectral component in Paper 1. Figure 4 shows how the spatial extent of an emission component varies with its velocity disperion and excitation classification. Broad, shocked emission in ULIRGs is usually spatially extended but is not detected as far away from the nucleus as is the narrow component. The broad, shocked component can typically be traced to ~ 5 kpc away from the peak continuum emission and up to 6 kpc in IRAS 03158+4227. We discuss the source of these broad, shocked outflows in Section 4.

4. OUTFLOW SOURCE

In general, the broad emission components are blueshifted to high velocity relative to the systemic velocity and only a few components are redshifted as shown in Fig. 3. For emission, a blueshifted line profile can be interpreted in two ways – outflow on the near side of the galaxy or inflow on the far side of the galaxy. In the case of dusty ULIRGs, however, the presence of dust obscuration allows a unique identification of the blueshift as outflow; photons coming from infalling gas on the far side of the galaxy would have a longer path length through dusty regions, thereby increasing the amoung of extinction. The outflow interpretation is further supported by the spatial extent of the blueshifted lines identified in Fig. 4. The spatial extent of broad blueshifted emission suggests that the emission is associated with regions beyond the deepest part of the gravitational potential well. In the following sections, we explore the possible physical origins of the outflow.

4.1. *Star Formation vs. AGN as a Power Source*

The power source of ULIRGs has been under debate for more than 20 years, owing to the obscuration in optical and shorter wavelengths by dust. Using the Spitzer Infrared Spectrograph (IRS), Veilleux et al. (2009) examined the power source of 14 of the 39 ULIRGs included in the Paper I sample by measuring indicators of AGN contribution from infrared indicators. Indicators of the strength of AGN contributions come from ratios of mid infrared emission lines [O IV]/[Ne II] and [Ne V]/[Ne II] (Armus et al. 2004, 2006, 2007; Veilleux et al. 2009), however, these ratios are well constrained for only 3 of the 14 ULIRGs in this sample. Two of the objects with well constrained contributions (IRAS01572+0009, IRAS12072-0444) show $\sim$ 90% AGN contributions to $L_{\rm bol}$. The third object (IRAS15001+1433) that is well constrained shows an $\sim$ 50% AGN contribution. Measurements of the mid-IR line ratios for the other 11 ULIRGs place a $\lesssim$ 30% upper limit on the AGN contribution to their bolometric luminosity. Although the AGN is generally not the dominant source of luminosity in these ULIRGs, we still need to investigate whether the broad lines could be directly related to the AGN.

4.1.1. *AGN Broad Line Region*

A broad line region (BLR) is a common feature in Seyfert 1 and 1.5 galaxies, appearing as permitted and intercombination emission lines broadened to 1,000 to 25,000 $\mathrm{km\,s^{-1}}$ FWHM (Osterbrock & Ferland 2006). The weakness of forbidden transitions in the BLR is explained by the high electron density, $n_e > 10^9\ \mathrm{cm^{-3}}$, which enhances collisional de-excitation (Peterson 2006). Reverberation mapping places the BLR size at much less than 1 pc (Bentz et al. 2009; Brewer et al. 2011), suggesting fast moving gas reflects the deep gravitational potential in the vicinity of a supermassive black hole (Dietrich et al. 1999). In our ULIRG spectra, emission from an AGN BLR would be confined to the central aperture ($\sim 1''$).

In the ULIRG spectra, however, the broad emission lines extend beyond a spatial resolution element, calling into question the BLR as a source of these features. Additionally the broad emission features appear not only in the permitted transitions, but also in the forbidden transitions. These observations, along with the low electron density measurements $\lesssim 100\ \mathrm{cm^{-3}}$ from [S II] line ratios, rule out an AGN BLR as the source of the broad, shocked emission components.

4.1.2. *Narrow Line Region*

In the emission-line ratio diagrams, we use the line defining the maximum excitation via extreme star formation (Kewley et al. 2006) to distinguish HII emission from shock-like emission. Above this, line ratios are typically attributed to narrow line regions of Seyfert galaxies or LINERs. The Seyfert and LINER line ratios can be described by fast shocks where the gas density ahead of the shock determines the influence of the radiative precursor on the overall emission line ratio. Gas rich Seyfert galaxies have a larger contribution from the radiative precursor, resulting in larger [O III]/Hβ ratios. LINERs are suspected to have lower gas densities ahead of the shock, which leads to lower [O III]/Hβ ratios (Dopita & Sutherland 1995).

The size of shocked AGN NLR region is empirically related to the luminosity of the [O III] λ5007 emission (Bennert et al. 2002; Greene et al. 2011). The scaling relation we use (Greene et al. 2011) is developed without corrections for in situ dust extinction of $L_{\rm [OIII]}$, owing to the difficulty of robust corrections for obscured quasars (Reyes et al. 2008). The [O III] luminosities ($L_{\rm [OIII]}$) used in this scaling relation, only includes spectral components where log([O III]/Hβ) is greater than 0.5 to avoid flux contributions from an HII region. For each galaxy, we estimate $L_{\rm [OIII]}$ from the broad, shock-like components and predict the expected size of an AGN NLR.

Since any nucleus can host an AGN, we measure luminosity for each galaxy in the pairs of merging galaxies – increasing the total galaxy count in this study to 48. Of the galaxies with components that have log([O III]/Hβ) > 0.5, the range of luminosities spans several orders of magnitude ($1.9 \times 10^{37} < L_{\rm [OIII]} < 3.2 \times 10^{42}\ \mathrm{erg\ s^{-1}}$) with a median $L_{\rm [OIII]} = 8 \times 10^{39}\ \mathrm{erg\ s^{-1}}$. For 9 galaxies (in 7 ULIRGs – IRAS00188-0586, IRAS01003-2238, IRAS05246+0103, IRAS08311-2459, IRAS09583+4714, IRAS13451+1232, and IRAS15130-1958) the measured outflow radii are within a factor of 1.6 of inferred radii from the scaling relation.

The majority of galaxies have $L_{\rm [OIII]}$ and spatial distributions that do not suggest excitation via AGN. In the 8 ULIRGs (13 galaxies), no components appear above the log([O III]/Hβ) > 0.5 cutoff, but we still detect shock-like line ratios up to 6 kpc from the closest nucleus, suggesting some other mechanism is responsible for the ionization. In 14 of these galaxies the components with appropriate log([OIII]/Hβ) appear only in regions outside the nuclear aperture. Galaxies that have a strong extended AGN presence would more likely consist of a contiguous region that includes the nucleus, suggesting that these are also not part of an NLR. The remaining galaxies have regions with shocked gas at radii greater than the estimated NLR size by a factor of 2.

In general, most cases do not favor AGN as the source of the observed emission line profile and instead are consistent with shocks driven by stellar winds and supernovae, as indicated by the AGN fractions. With this understanding of the outflow source, we can make estimates of the outflowing masses and the energy injected into the system by these processes.

4.2. *Energetics of Supernova Feedback*

Excluding the AGN-dominanted cases IRAS01572+0009 and IRAS12072-0444, the star formation rates in these ULIRGs indicate enormous amounts of mechanical power is deposited in the ISM by massive stars. In this section, we compare mechanical power to the power in the bulk outflow of warm-ionized gas. We stress that our estimates of the mass and kinetic energy in the bulk flow are no better than factor of $\sim$ 3 accuracy. Uncertainty about the filling factor

TABLE 1
Outflow Parameters

IRAS Name (1)	L_{IR} (2)	v_{out} (3)	r_{out} (4)	t_{out} (5)	L_{tot} (6)	M_L (7)	M_Σ (8)	$\dot{M}_L$ (9)	$\dot{M}_\Sigma$ (10)	SFR (11)	η_L (12)	η_Σ (13)
IRAS00153+5454	12.10	270	3.71	13.31	51.5	17	47	1.3	3.6	68	0.02	0.05
IRAS00188-0856	12.33	660	1.57	2.32	407.	130	31	58	13	128	0.45	0.10
IRAS01003-2238	12.25	1140	3.66	3.13	203.	67	155	21	50	96	0.22	0.52
IRAS01298-0744	12.29	240	11.27	44.98	86.6	28	620	0.6	14	57	0.01	0.24
IRAS03158+4227	12.55	1330	7.22	5.30	181.	59	423	11	80	191	0.06	0.42
IRAS05246+0103	12.05	250	2.71	10.54	33.1	10	22	1	2.1	60	0.02	0.04
IRAS05246+0103	12.05	850	3.10	3.56	520.	170	110	48	31	60	0.80	0.52
IRAS08311-2459	12.40	600	4.94	8.08	338.	110	320	14	40	135	0.10	0.30
IRAS09111-1007	11.98	290	1.38	4.68	26.3	8	7.3	1.8	1.6	51	0.04	0.03
IRAS09583+4714	11.98	350	4.42	12.27	413.	140	320	11	26	51	0.20	0.50
IRAS10378+1109	12.23	1000	3.80	3.72	267.	88	150	24	41	92	0.26	0.45
IRAS10494+4424	12.15	730	4.34	5.78	80.2	26	88	4.6	15	76	0.06	0.20
IRAS10565+2448	11.98	250	2.66	10.54	23.2	8	29	0.7	2.8	66	0.01	0.04
IRAS11095-0238	12.20	260	3.65	13.61	145.	48	120	3.5	8.8	95	0.04	0.09
IRAS12071-0444	12.31	570	7.95	13.57	15.9	5	210	0.4	15	25	0.02	0.61
IRAS15130-1958	12.03	890	3.65	4.03	29.5	10	51	2.4	13	24	0.10	0.53
IRAS16090-0139	12.48	640	6.61	10.07	17.0	6	86	0.6	8.5	179	0.003	0.05
IRAS16487+5447	12.12	400	5.79	14.01	147.	49	360	3.5	26	71	0.05	0.36
IRAS17028+5817	12.11	200	1.33	6.42	121.	40	14	6.2	2.1	69	0.09	0.03
IRAS18368+3549	12.19	370	4.09	10.70	333.	110	140	10.	13	83	0.12	0.16
IRAS19297-0406	12.36	730	4.30	5.74	233.	77	180	13	31	123	0.11	0.25
IRAS20087-0308	12.39	330	5.62	16.48	1170	390	760	24	46	132	0.18	0.35
IRAS23327+2913	12.03	630	3.81	5.95	60.5	20	99	3.4	17	58	0.06	0.29
IRAS23365+3604	12.13	580	0.89	1.50	5.52	2	1.6	1.2	1.1	73	0.02	0.02

Note. — Column 1: IRAS Name. Column 2: Total infrared luminosity $\log(L_{IR}/L_\odot)$ (Murphy et al. 1996). Column 3: Outflow velocity taken as $v_{out} = |v| + \sigma_v$ (km s^{-1}) from the Paper I (Table 3). Since we are unsure of the degree to which projection effects play a role in the measured velocity, assume all outflowing regions have the same v_{out}, but is foreshortened. In this simplification we take the maximum v_{out} of the apertures, to represent the vector that is most parallel to the line of sight. Column 4: Maximum radius of outflow (kpc). r_{out} is defined by the maximum separation between an aperture which shows outflow and the continuum peak. Column 5: outflow time scale (Myr). Column 6: Total luminosity of Hα from the outflow components ($L_{tot}/10^{40}$) erg s^{-1}. We correct the Hα emission for Galactic dust extinction using the reddening curve from Cardelli et al. (1989) and values of E(B-V) and A_V from the Infrared Science Archive maps (Schlegel et al. 1998). We use the measured Balmer decrement and the Calzetti et al. (1994) reddening curve to correct for internal extinction. Column 7: Mass of outflowing gas in 10^6 M$_\odot$ from L_{tot} and Eq.4 assuming $n_e = 100$ cm^{-3} and $\gamma' = \gamma_{phot}$. Column 8: Mass of outflowing gas in 10^6 M$_\odot$ from Σ and Eq.6 with an assumed hemisphere geometry, with the maximum path length through the sphere defined by the radius, $\delta s = r_{out}$, and $f = 0.01$. Within each aperture the path length through the sphere varies as $s = (r_{out}^2 - (r_{aperture} - r_{nucleus})^2)^{1/2}$ Column 9: Outflow rate estimated from L_{tot} in M$_\odot$ yr^{-1} described in Section 4.2.2. Column 10: Outflow rate estimated from Σ in M$_\odot$ yr^{-1} with an assumed hemisphere geometry. Column 11: Star formation rate estimated from L_{IR} are values (Murphy et al. 1996) and relation SFR = $L_{IR}/13.0 \times 10^9 L_\odot$. This relation is an adjustment of the Kennicutt (1998) relation adjusted for a stellar mass range from 1 to 100 M$_\odot$ (M$_\odot$ yr^{-1}). This star formation rate is also corrected for AGN contribution to L_{bol} for the objects included in Veilleux et al. (2009). In cases where upper limits to the AGN fraction are not provided for an individual object in Veilleux et al. (2009), we use the average AGN contribution of 30%. Column 12: Efficiency of outflow from $\dot{M}_L$. Column 13: Efficiency of outflow from $\dot{M}_\Sigma$ with an assumed hemisphere geometry and filling factor $f = 0.01$. The objects in this table are restricted to those that have at least 1 aperture with a shock- like spectral component with $\sigma_v > 150$ km s^{-1}.

of the warm-ionized gas and the large-scale geometry of the outflow dominate the systematic error. The mass, energy, and momentum carried by the outflowing, warm-ionized gas should clearly be viewed as a lower limit on the total amounts carried by all phases of the wind, which likely includes substantial components of both coronal gas and molecular gas.

4.2.1. *Mass of Warm-Ionized Gas*

For each ULIRG that shows broad, shock-like emission components, we can estimate the outflowing mass of warm-ionized gas. This mass is the product of the gas density and the volume occupied by the warm-ionized phase.

The fraction of the total volume V filled with warm-ionized gas is called the filling factor. For HII regions, this filling factor,

$$f \equiv \frac{\langle n_e^2 \rangle}{n_e^2}, \tag{1}$$

is computed from the RMS electron density obtained from the Hα luminosity or surface brightness and the electron density computed from a density-sensitive doublet ratio such as [S II] $\lambda\lambda 6717, 31$. Values of the filling factor range from $0.001 < f < 0.1$ in nearby HII regions (Searle 1971; Kennicutt 1984; Kaufman et al. 1987) and therefore have a very signficant impact on the estimated mass. The range of filling factor may indeed be different in the ULIRGs, given the difference in star formation rate from these HII regions in normal galaxies, but these values provide a point of comparison. In the ULIRG spectra, the flux ratio for the [S II] doublet is typically consistent with the low-density limit and indicates $n_e \lesssim 100$ cm^{-3}, but the ratios of the two [S II] lines indicate densities $n_e \approx 500$ cm^{-3} in the central apertures of IRAS01003-2238, IRAS05246+0103, IRAS08311-2459, IRAS09583+4714, and IRAS23327+2913. For our mass estimates, we adopt a fiducial value of $n_e = 100$ cm^{-3} but carry along the scaling with density explicitly in our results.

The outflow mass is

$$M_{out} = \mu m_H V n_e f, \tag{2}$$

where n_e is the electron density, m_H is the mass of hydrogen, and the mass per H atom is $\mu = 1.4$ amu when helium is included. The unknown factor Vn_ef in Eqn. 2 is simply related to the Hα luminosity by

$$\mathrm{L}_{\mathrm{H}\alpha} = \gamma' \left\langle n_e^2 \right\rangle \mathrm{V} = \gamma' n_e^2 f \mathrm{V}. \tag{3}$$

Eliminating the common factor between Eqn. 2 and 3, the outflowing mass,

$$M_{\mathrm{L}} = \frac{\mu \mathrm{m_H} \mathrm{L}_{\mathrm{H}\alpha}}{\gamma' n_e}, \tag{4}$$

can be estimated from the luminosity of the broad, shocked emission component for any assumed value of the gas density, n_e.

The effective volume emissivity, γ', varies depending on the temperature and excitation mechanism. For photoionized regions with T = 10^4 K, $\gamma' = \gamma_{\mathrm{phot}} = \alpha^{\mathrm{eff}}_{\mathrm{H}\alpha} \mathrm{h}\nu = 3.56 \times 10^{-25}$ erg cm^3 s^{-1} in Case B recombination theory (Osterbrock & Ferland 2006). In shocked regions, collisional excitation and ionization can make γ' larger or smaller than γ_{phot} by a factor of two to three (Goerdt et al. 2010; Genzel et al. 2011). Since the photionization case is in the middle of the plausible range for γ_{phot}, we estimate masses using γ_{phot}.

We present the estimated masses in Table 1. They range from 1.8×10^6 M$_\odot$ to 3.9×10^8 M$_\odot$. The median and standard deviations are 40×10^6 M$_\odot$ and 84×10^6 M$_\odot$ respectively. The systematic errors in the mass estimate are difficult to quantify. For example, Fig. 5 illustrates the aperture correction to the observed flux. In addition, corrections for internal Hα extinction can be large. The large outflow mass in IRAS20087-0308, for example, is due in large part to the extinction correction. For individual galaxies, the masses in Col. 7 of Table 1 should be interpreted as rough estimates accurate to a factor of 2-3.

The measured Hα surface brightness provides a sanity check on the assumed electron density, or equivalently $\left\langle n_e^2 \right\rangle^{1/2} f^{-1/2}$ by Eqn. 1. The Hα surface brightness, $\Sigma = L_{Ha}/A$ depends on the three-dimensional shape of the outflow since the volume is the product of the projected area A and the depth of the emitting region, Δs, along the sightline. The surface brightness depends on density as

$$\Sigma = \left\langle n_e^2 \right\rangle \gamma' \Delta s \tag{5}$$

By analogy to Eqn. 4, the inferred outflow mass is

$$M_\Sigma = \left(\frac{\mu m_H A \Sigma}{\gamma' n_e} \right) = \mu m_H L \left(\frac{\Delta s f}{\gamma' \Sigma} \right)^{\frac{1}{2}}. \tag{6}$$

In Table 1, col. 8 provides examples of the mass estimates obtained by this method.

If our density estimate n_e is reasonable, then equating M_Σ and M_L should imply reasonable values for the product of the filling factor and the depth of the emitting region along the line of sight. If we adopt $f = 0.01$, then the required path length through the emitting region is often only a few hundred pc. Such a small pathlength would arise only if the emitting region had a hollow shell structure. If the emitting region is roughly spherical, $\Delta s \approx \sqrt{A}$, the implied filling factor is often small, $f \sim 10^{-3}$. The real values of s and f that unify the mass estimates may involve a change in both of these parameters, but will depend on each individual case. The bottom line is the volume filling factor of the warm-ionized gas may be tiny thereby leaving lots of volume to be filled by gas at a different temperature.

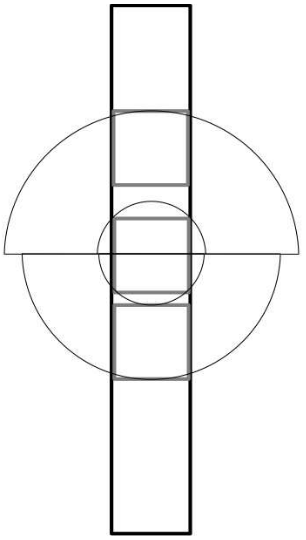

FIG. 5.— The long black rectangle represents the slit, the gray boxes represent apertures along the slit, the annuli are the total estimated regions for each position. The number of outflows detected in ULIRGs (75-80% Rupke et al. 2002; Martin 2005) suggests that a biconical outflow cone has a large opening angle ∼145°. This allows us to use a sphere as a rough approximation to the geometry. We estimate the luminosity contributed by regions outside of the slit by assuming this circular symmetry and a constant surface brightness within the half annuli as the aperture within it. The central aperture coincides with the nucleus of the galaxy used in the measurement.

4.2.2. *Outflow Velocity and Time Scale*

The time scale for the outflow is estimated from the geometry and the kinematics measured from the emission line profile. In Table 1, we define the outflow velocity (v_{out}) as $|v| + \sigma_v$ (km s^{-1}) taken from Table 3 in Paper I. The median v_{out} in this sample is 580 km s^{-1}, and the values range from 200 to 1330 km s^{-1}.

Estimating the outflow timescale from the outflow radius and velocity, $t_{out} = r_{out}/v_{out}$, the implied mass loss rate of warm-ionized gas is $\dot{\mathrm{M}} = \mathrm{M_{out}}/\tau$. For the estimate of mass outflow using luminosity (M$_\mathrm{L}$), we find a range from 0.4 to 58 M$_\odot$ yr^{-1} where the median is 4.6 M$_\odot$ yr^{-1}. The largest $\dot{\mathrm{M}}$ is in IRAS00188-0856, due mostly to the moderate v$_{\mathrm{out}}$ and small r$_{\mathrm{out}}$. The surface brightness mass estimate with a spherical geometry (M$_\Sigma$) gives larger outflow rates on average from 1 to 80 M$_\odot$ yr^{-1} where the median is 15.2 M$_\odot$ yr^{-1}. In this case the largest outflow rate is in IRAS03158+4227, which has a large v$_{\mathrm{out}}$ and r$_{\mathrm{out}}$, but in the surface brightness case, the large r$_{\mathrm{out}}$ has a greater influence.

4.2.3. *$\dot{M}$ vs SFR*

An important parameter in modeling galactic winds is the efficiency (η) that star forming regions are able to remove gas from the star forming region. This parameter informs the timescale over which a galaxy will form stars before the stellar population itself removes gas and shuts down star formation. We estimate η as the ratio of outflow mass to the star formation rate measured from IR luminosities in Murphy et al. (1996) (Table 1). We use the star formation rate estimated from the SFR = $L_{IR}/13.0\times10^{9}L_{\odot}$ (Kennicutt 1998), adjusted for a stellar mass range from 1 to 100 $M_{\odot}$ and correcting the L_{IR} for the AGN fraction.

In this sample of galaxies, the outflow rates typically yield $\eta \sim 10^{-1}$ but span the range $10^{-3} < \eta < 1$. We emphasize, however, that this measurement refers only to the warm ionized gas, which may be the dominant phase of the outflowing gas. The mass outflow rates in the cool gas traced by Na I are at least a few tenths of the star-formation rate, $\eta \equiv \dot{M}/SFR \approx 0.1$, but are poorly constrained due to the large variations in ionization parameter among ULIRGs (Martin 2005; Murray et al. 2007). Hot winds and molecular outflows may also carry significant mass.

4.2.4. *Shock Energetics*

The presence of outflows implies that mechanical energy is injected into the gas. For objects that show outflow in emission, we can estimate the energy injection rate into the gas from a starburst by using the star formation rate. We scale the predicted supernova energy injection rates from (Leitherer et al. 1999, SB99) to the calculated SFR for each source, after correcting for differences in the assumed IMF low mass cutoff (Kennicutt 0.1 - 100 $M_{\odot}$, SB99 1-100 $M_{\odot}$). We assume continuous star formation model over a timescale longer than 40 Myr. This produces a nearly continuous injection of feedback energy contributed by supernovae and stellar winds.

The simplest model for the initial response of the interstellar gas to this feedback is based on stellar wind bubbles (Weaver et al. 1977; Shull & McKee 1979). Shocks direct 55% of the feedback energy into the thermal energy of low density, coronal bubble and the other 45% into an expanding shell of swept-up interstellar medium. About 60% of the shell energy is radiated away in this model, suggesting that luminosity of the shocks would be 27% of the feedback power. For typical shock velocities, most of this energy will come out in ultraviolet and optical emission lines. The energy in the optical lines will be slightly greater than the UV lines by $\sim$ 20%, suggesting that $\sim$ 15% of the feedback power will come out in optical emission (Shull & McKee 1979).

Using our estimates of physical properties in Section 4.2.1 and the shock speeds from Paper I, we can make comparisons to these efficiencies. In Figure 6 we show the ratio of the total optical luminosity (L_{opt}) for the components indicating shocked outflowing gas in the measured lines compared to the mechanical power (L_{w}, inferred from the SFR). Since the luminosity of the optical emission lines is generally less than $\sim$15%, it follows that supernova feedback is a plausible source of power for this shocked emission.

Luminosity in the optical emission lines for 4 of the galaxies (IRAS05246+0103, IRAS09583+4714, IRAS13451+1232, and IRAS20087-0308) exceeds the expected fraction of energy injected into outflow by supernovae. The excess emission line energy in these objects (except for IRAS20087-0308), may be due to additional emission from an AGN NLR, since for these objects, the emission region size from scaling relations is consistent with that of an AGN NLR. Emission from IRAS20087-0308 encounters heavy extinction making the Balmer decrement difficult to measure, resulting in a possible over correction to the extinction, which would then skew the L_{opt}/L_{w} ratio.

We calculate the ratio of power that appears as kinetic energy from the outflow rate (L_{KE}) to the mechanical energy injection rate from the estimated mass and velocities measured for the outflow regions in Table 1. This kinetic energy estimate uses $\dot{M}_{L}$ as the outflow mass estimate and v_{out} for the velocity. In Figure 6, we show that this energy rate is again consistent with the fraction of energy in outflow models (mean = 0.08), which predict a $\sim$ 20% fraction of mechanical energy in the kinetic energy of the shell. The consistency in kinetic energy fraction with the models suggests that this process is possibly at work driving the outflows in ULIRGs. It also implies that the estimated masses are correct within an order of magnitude.

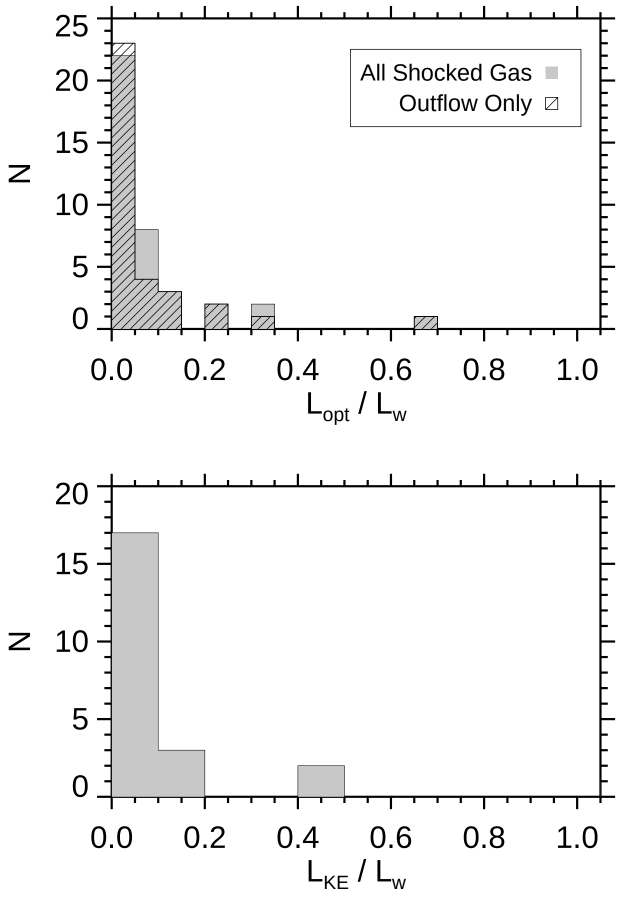

FIG. 6.— *above:* A histogram showing the measured luminosity (L_{opt}) emitted in shocked gas compared to the mechanical energy injection rate (L_{w}) from supernovae scaled from the IR star formation rate with SB99. For a whole galaxy, both the emission associated with the shocked outflow (hashed) and the emission from all shocked regions (solid) are generally in the range 0 - 15%, with the peak below 5%. The measured values are consistent with Weaver et al. (1977). *below:* The fraction of the feedback energy that contributes the kinetic energy in the mass outflow is again consistent with the Weaver model.

5. DISCUSSION

5.1. *Outflows in Integrated Spectra*

In observations of galaxies at high redshift, obtaining similar spatial resolution to this study is difficult due to the small angular size of galaxies. The degree to which spatially integrated emission lines show evidence for the outflows in these spectra is unclear. We examine spatially integrated spectra in these data to examine which of the resolved features remain evident in the integrated spectra.

5.1.1. *Spectral Classifications from the Total Line Flux*

In low spectral resolution, spatially unresolved studies of galaxies, one means of examining the excitation mechanism is through total line flux classifications. We apply the same classifications (Paper I) to the ULIRGs based on spectra obtained by integrating along the slit. These total line flux classifications may be influenced by the observed shocks in outflows and gas disks. We examine the relation between classification and the presence of these shocks to determine which of the Seyferts, LINERS, and HII classified galaxies host shocked gas.

All 6 galaxies classified as Seyferts present broad, blueshifted outflows in the kpc scale apertures. The narrow emission line components in these Seyferts also present shock-like ratios in four out of six cases – IRAS00188-0856, IRAS01003-2238, IRAS13451+1232, and IRAS15130-1958. These four Seyfert galaxies have both narrow and broad emission components that present shock-like flux ratios. The luminosity of the broad, shocked component is sufficient $L_{[OIII]}$ to generate a spatially resovled NLR. We conclude AGN photoionization is the source of excitation for these four galaxies.

IRAS09583+4714 and IRAS12071-0444 present the two exceptions for the Seyfert classified galaxies, where the broad components differ from the narrow components in their excitation. Of the two galaxies in the double IRAS09583+4714, the galaxy with shocked outflow presents narrow component excitation consistent with HII and has a strong, disk-like rotation gradient. In IRAS12071-0444, the narrow components have excitation more consistent with a LINER classification and are highly extended to ±9 kpc. For both of these exceptional galaxies, scaling relations from $L_{[OIII]}$ suggest that the outflow region is larger than what would be expected from an AGN NLR. The inconsistency of the outflow excitation with the integrated classification in these two galaxies suggest that a significant fraction of ULIRGs may be misclassified as Seyfert galaxies, when they host shocks in outflows outflows driven by star formation.

The subset of 9 galaxies classified as LINERs frequently host both narrow, shocked components and broad, shocked components. In all but one of these objects, narrow, shocked emission appears least 5 kpc from their associated nucleus. Among the 6 LINER spectra with broad, shocked components, the outflow is spatially extended in 5 of them. None of the 9 galaxies have sufficient $L_{[OIII]}$ to suggest that the shocked outflow or the narrow, shocked component is powered by an AGN NLR. These examples emphasize that a integrated galaxy spectrum with a LINER classification need not indicate the presence of an AGN.

Among the sample, 12 galaxies had emission line ratios on the borderline between classifications. Six of these borderline galaxies have ratios between the Seyfert and LINER classifications. These six galaxies have broad outflows as well as extended shocks that are not part of the bulk outflow. The two borderline galaxies with classifications between HII and LINER do not host shocked outflows, but do have extended shocks, which is responsible for making the net classification slightly outside the range of the HII galaxies. the last of these twelve galaxies are a mix of classifications, without a clear trend in behavior.

The largest fraction of the sample (21 out of 48 galaxies) is classified as HII in the integrated spectra. These galaxies share the same HII classification in the diagnostic diagrams that compare [O I]/Ha and [S II]/Hα, but the [N II]/Hα can be either HII or "composite" as described in Kewley et al. (2006). The subset of galaxies with a "composite" classification are also host to either shocked outflows or shocks in the extended narrow emission line gas. Clearly, the presence of shocks in these objects modifies the [N II]/Hα classification, but observations with kpc scale spatial resolution showed that supernovae are a plausible source of the forbidden line enhancement and the outflow.

The spatially resolved analysis was also aided by the simultaneous multiple component fit to the emission line profiles, so we next investigate the integrated spectrum with the multiple component fit.

5.1.2. *Identifying Shocks in the Integrated Spectral Profiles*

Our analysis of spatially and spectrally resolved line emission provides new insight on how to identify regions of shocked gas. Here, we examine whether the method works on integrated spectra with moderate spectral resolution. This analysis differs from the previous section by comparing the line shapes in the integrated profiles to those in the apertures.

This analysis allows us to define the required ranges and resolutions of instruments obtaining the integrated spectra. Clearly, the integrated spectra must cover [O I]λ6300. The strong [O I]λ6300 emission from shocked regions and the separation of this transition from other lines make it critical for uniquely fitting multiple velocity components. Furthermore, we will assume the integrated spectra have spectral resolution of at least $R \geq 5000$ and signal to noise $\sim$ 15 if multi-component fitting will be attempted.

Of the 24 galaxies that exhibit broad blueshifted outflow in the spatially resolved analysis, 19 galaxies also show these features in the integrated spectrum. In the remaining 5 galaxies, the strong narrow lines observed in the resolved analysis mask the signature of broad outflow in the integrated spectrum.

Regions with narrow ($\sigma_v < 150$ km s^{-1}) emission lines that have shock-like line ratios appear frequently (34 of 48 galaxies) in the spatially resolved analysis. Over a large range in position, these narrow features are identified at Doppler shifts ranging from -250 km s^{-1}to 250 km s^{-1}in a few galaxies. Averaging over a large range in Doppler shift acts to broaden the integrated line profiles. In 5 of the 34 galaxies with narrow shock emission, the summed components form a line of width $\sigma_v > 150$ km s^{-1} in the integrated spectrum. These galaxies are mostly classified as HII with flux ratios in the "composite" region of the [N II]/Hα vs [O III]/Hβ diag-

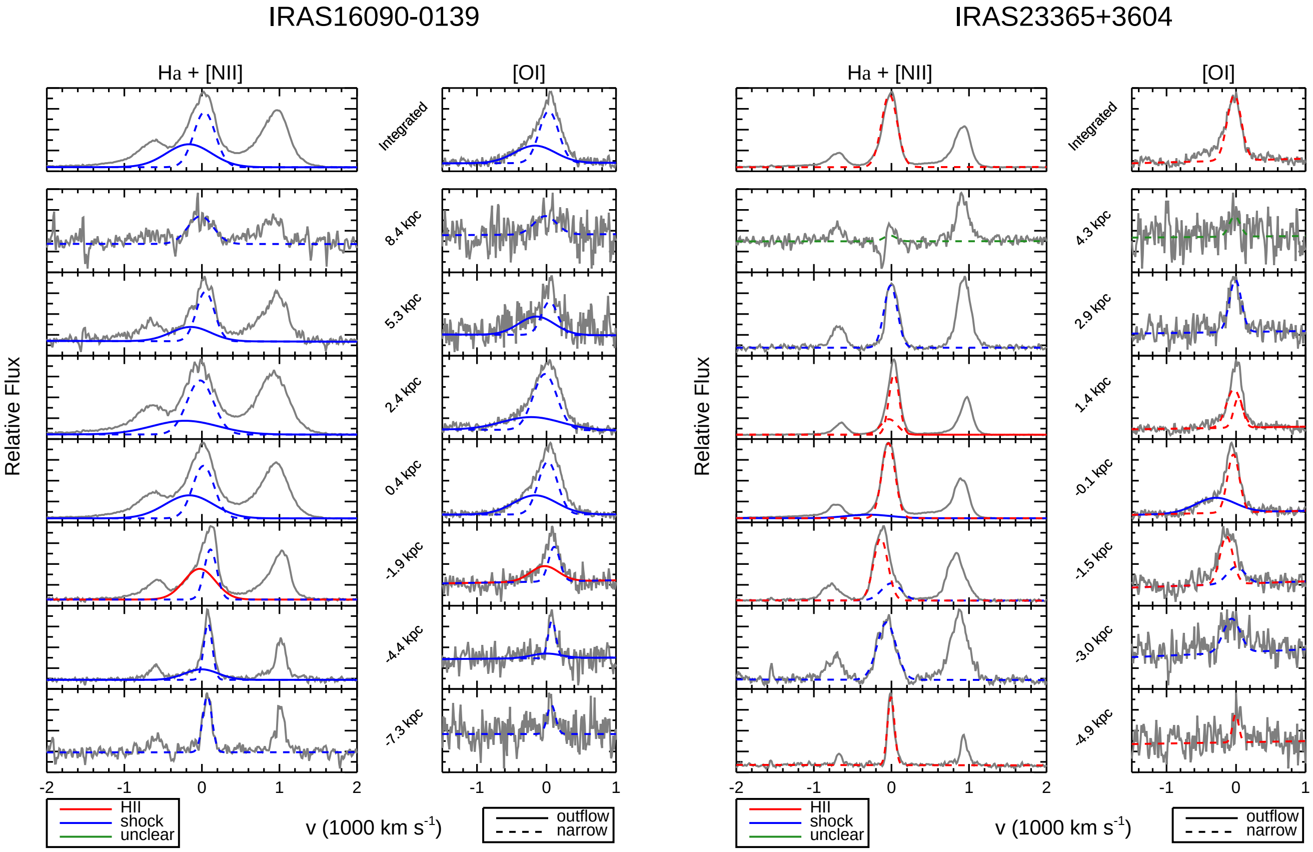

FIG. 7.— Plot of the Hα+[N II] and [O I] regions of the spectrum for both the integrated apertures and the spatially resolved apertures for IRAS16090-0139 and IRAS23365+3604. Line color represents the excitation classification of each component into "HII" (red), "Shock-like" (blue), "unclear" (green). The line style identified the components that are part of an identified outflow (solid), compared to the rest of the emission components (dashed). *L*eft: IRAS16090-0139 presents outflow components in the resolved analysis that also appears in the integrated spectrum. The observed narrow shock also appears in the integrated profile fit. *R*ight: In the nuclear aperture of IRAS23365+3604 we identify outflow from the kinematics in the emission component. The apertures at 2.9 kpc and 3 kpc from the continuum source identify emission from shocked gas. All of these features are washed out in the integrated profile.

nostic diagram. Fig. 7 shows the integrated aperture and spatially resolved apertures for IRAS16090-0139, which exhibits the outflow and narrow shocks from the resolved analysis in the integrated profile. We also compare this to the case of IRAS23365+3604, which shows both types of shock in the spatially resolved analysis, while the integrated case is only identified as HII.

In 15 out of the 34 galaxies, the Doppler shifts of the narrow, shocked components span a small enough range to be detected as 'narrow, shocked' components in the integrated spectrum. A narrow span of Doppler shifts would also make any broad outflow more identifiable, which means that objects with low inclination gas disks will show broad outflows more often.

We conclude that applying the multiple component fitting technique to integrated spectra would have some success in identifying broad, shocked components from outflows. In our sample, the outflow is undetected in the integrated spectrum only 20% of the time. In these 5 failures, a broad component is in fact detected in the integrated spectrum; but the spatially resolved analysis indicates the emission comes from a gas rotating like a disk. Building a better understanding of the physical origin of the narrow, shock-like emission component is therefore critical for interpreting the presence of broad, shocked emission in integrated spectra.

5.2. *Lessons From the Local Laboratories*

While there are important differences between ULIRGs and star-forming disks at $z > 2$, ULIRGs present high specific star formation rates that are similar to the high end of starforming galaxies from $2.5 < z < 5$ (Elbaz et al. 2007; Cunha et al. 2010; Feulner et al. 2005). The similar specific star formation rates suggest that local ULIRGs can provide insight into processes that occur below current resolution limits and that the broad emission components may share a common origin. Using adaptive optics (AO) spectroscopy of $z \sim 2$ galaxies, star-forming clumps were recently shown to be the origin of the broad Hα/[N II] line wings (Genzel et al. 2011). The $\sim$ 4 kpc offset of these clumps from the galactic center suggests a supernova-driven outflow, rather than an AGN, broadens the line emission. The more central location of the broad emission found in the ULIRGs illustrates that the ULIRGs are not direct analogs of the $z \sim 2$ galaxies but the radius and luminosity of the broad emission region in most of these ULIRGs is uncomfortably large to be caused by the AGN.

In the echellete spectra, broad emission features are identified in the line profiles through the simultaneous fitting of multiple transitions. Our fitted linewidths are not as large as the broad Hα/[N II] wings reported for $z \sim 2$ galaxies (Shapiro et al. 2009) because our spectra require broad components in the forbidden lines as well as the recombination lines. Additionally, since ULIRGs are known to be much more reddened than the $z \sim 2$ starbursts; broad emission-line profiles produced by similar physical processes in the less-dusty $z \sim 2$ galaxies will be more symmetric with respect to the systemic velocity and therefore broader than those in ULIRGs. While Shapiro et al. (2009) had difficulty distinguishing a BLRs and superwinds as a source of the broad emission features identified in stacks of $z \sim 2$ spectra, the simultaneous fitting of more broad forbidden lines allows the identification of other sources of the broad emission rather than just Hα.

The estimates of outflow mass and outflow rate in the local ULIRGs provides context to the estimates of outflow rate and mass in the starforming clumps at $z \sim 2$ (Genzel et al. 2011). The star formation rate in these local ULIRGs (24 - 180 $\mathrm{M}_\odot$ yr^{-1}) is much greater than the star formation rate in the $z \sim 2$ starforming clumps (3.3 to 40 $\mathrm{M}_\odot$ yr^{-1}), but our estimates of the mass outflow rate are much lower (0.4 to 58 $\mathrm{M}_\odot$ yr^{-1} for ULIRGs, 6 to 200 $\mathrm{M}_\odot$ yr^{-1} for starforming clumps). These results are consistent with a higher η for warm ionized gas at high redshift but do not demand it. The gas density or the filling factor adopted for the high redshift galaxies could be tuned to give results for η similar to what we infer for these ULIRGs.

Some properties of these outflows are easier to study in nearby galaxies, and the methods in this study illustrates how more information about the outflows at $z \sim 2$ can be obtained, even in integrated spectra. As mentioned already, for example, the outflows in $z \sim 2$ galaxies likely have shock-like line ratios similar to those in our ULIRG sample. The properties of these shocks can be estimated once spectral coverage of additional lines – particularly [O I], Hβ, and [O III] – are obtained at moderate spectral resolution, $R \approx 5000$, with similar signal to noise (~ 15) as in this study.

6. SUMMARY

Paper I mapped optical, emission-line ratios across 39 ultraluminous infrared galaxies in 2 dimensions, i.e., line-of-sight velocity plus one spatial dimension. In this paper, we have used those measurements to describe the kinematics of regions excited by different physical processes. Figure 2 shows the distribution of line-of-sight velocity dispersion for regions with shock-like and HII-like line ratios. The median linewidth for the shock-like components, $\sigma_v \approx 144$ km s^{-1}, is higher than that of the HII-like components, 61 km s^{-1}. The difference is caused by the large number of shock-like components broader than $\sigma_v \approx 150$ km s^{-1}and the near absence of HII-like components with linewidths this large.

These broad emission components are relevant to our understanding of gas inflows and outflows because gas in virial equilibrium would produce lines with smaller widths. Our results provide insight into the interpretation of the emission-line spectra of high redshift galaxies, particularly dusty galaxies with extremely high star formation rates.

We find that the broad shock-like components are typically spatially extended, reaching radii up to 6 kpc in Figure 4. We show that in 9 out of 24 broad components, the size of this region exceeds that expected for an AGN NLR under the assumption that [OIII] 5007 luminosity from components with $\log([\mathrm{O\ III}]/\mathrm{H}\beta) > 0.5$ is powered by the AGN. We estimate the total power radiated by summing the optical luminosities of the broad line components and applying a geometrical correction for slit losses. Since the resulting shock luminosities range from 5-20% of the mechanical power from supernova explosions, we conclude that supernovae are a viable power source for the gas flows that generate the shocks.

In ultraluminous *infrared* galaxies, dust absorbs much of the starlight; and the centers of these galaxies are not transparent at ultraviolet and optical wavelengths. At least in the central few kpc, we can be reasonably certain that the emergent emission-line profile is shaped by gas on the near side of the galaxy. We therefore interpret the blueshifts of the broad components as direct evidence that the gas is outflowing. In less dusty galaxies, this outflow component would presumably also have a red wing from emission coming from the far side of the galaxy.

The broad components have surprisingly smooth line profiles. Across luminous infrared galaxies with winds, for example, the Hα + [NII] profiles are well described by a single, Gaussian component where emission from HII regions in the underlying disk dominate the flux. When the outflows are observed against the sky, along the minor axis, the emission lines are typically double peaked (Lehnert & Heckman 1995). The relative intensities of the two components have been shown to reflect the inclination and opening angle of a biconical outflow (Heckman et al. 1990). That some of the broad emission is detected beyond the continuum emission in these ULIRGs, yet does not have a double-peaked profile may be related in part to the obscuration of the back side of the outflow. However, it is not obvious that the galaxies are opaque at these large radii, and we tenatively conclude that the warm-ionized, outflowing gas in ULIRGs does not share the biconical structure that describes outflows in LIRGs very well.

The prominence of shock-excited emission in these starburst galaxies raises questions about how shocked emission skews the emission-line ratios measured from integrated spectra. Since the luminosity in the ultraviolet, ionizing continuum exceeds the mechanical power from supernova and stellar winds by about an order of magnitude (Leitherer et al. 1999; Martin 2007), we would not expect shocks from galactic winds to determine the line ratios measured in integrated spectra. What Figure 8 clearly demonstrates, however, is that when integrated spectra have moderately high spectral resolution, $R \sim 5000$, shocked, outflowing gas can sometimes be recognized by comparing the line profiles of forbidden lines, particularly [OI] 6300, to the blended Hα + [NII] profile. We conclude that multi-component line fitting of at least these 4 transitions in the rest-frame optical spectrum can provide useful diagnostics of shock velocities and radiative energy losses in galaxies over a very broad range of cosmic time.

The authors thank Kristian Finlator, Nicolas Bouché, Alaina Henry, Vardha Bennert, Tommaso Treu, and Omer Blaes for illuminating discussions. This work was supported by the National Science Foundation under contracts AST-0909182 and AST-1109288 and the Department of Education through the Graduate Assistance in Areas of National Need program. A portion of this work was completed at the Aspen Center for Physics. The authors wish to recognize and acknowledge the very significant cultural role and reverence that the summit of Mauna Kea has always had within the the indigenous Hawaiian community. We are most fortunate to have the opportunity to conduct observations from this mountain.

Facilities: Keck

REFERENCES

Armus, L., Heckman, T. M., & Miley, G. K. 1990, Astrophysical Journal, 364, 471

Armus, L., et al. 2004, The Astrophysical Journal Supplement Series, 154, 178

—. 2006, The Astrophysical Journal, 640, 204

—. 2007, The Astrophysical Journal, 656, 148

Bennert, N., Falcke, H., Schulz, H., Wilson, A. S., & Wills, B. J. 2002, The Astrophysical Journal, 574, L105

Bennert, N., Jungwiert, B., Komossa, S., Haas, M., & Chini, R. 2006a, Astronomy and Astrophysics, 459, 55

—. 2006b, Astronomy and Astrophysics, 456, 953

Bentz, M. C., et al. 2009, The Astrophysical Journal, 705, 199

Borne, K. D., et al. 1999, Astrophysics and Space Science, 266, 137

Brewer, B. J., et al. 2011, The Astrophysical Journal Letters, 733, L33

Calzetti, D., Kinney, A. L., & Storchi-Bergmann, T. 1994, The Astrophysical Journal, 429, 582

Cardelli, J. A., Clayton, G. C., & Mathis, J. S. 1989, Astrophysical Journal, 345, 245

Cunha, E. D., Charmandaris, V., Díaz-Santos, T., Armus, L., Marshall, J. A., & Elbaz, D. 2010, Astronomy and Astrophysics, 523, 78

Daddi, E., et al. 2007, The Astrophysical Journal, 670, 156

Dasyra, K. M., et al. 2006, The Astrophysical Journal, 638, 745

Dietrich, M., Wagner, S. J., Courvoisier, T. J.-L., Bock, H., & North, P. 1999, Astronomy and Astrophysics, 351, 31

Dopita, M. A., & Sutherland, R. S. 1995, Astrophysical Journal v.455, 455, 468

Elbaz, D., et al. 2007, Astronomy and Astrophysics, 468, 33

Feulner, G., Gabasch, A., Salvato, M., Drory, N., Hopp, U., & Bender, R. 2005, The Astrophysical Journal, 633, L9

Genzel, R., Tacconi, L. J., Rigopoulou, D., Lutz, D., & Tecza, M. 2001, The Astrophysical Journal, 563, 527

Genzel, R., et al. 2011, The Astrophysical Journal, 733, 101

Goerdt, T., Dekel, A., Sternberg, A., Ceverino, D., Teyssier, R., & Primack, J. R. 2010, Monthly Notices of the Royal Astronomical Society, 407, 613

Gonçalves, T. S., et al. 2010, The Astrophysical Journal, 724, 1373

Greene, J. E., Zakamska, N. L., Ho, L. C., & Barth, A. J. 2011, The Astrophysical Journal, 732, 9

Heckman, T. M., Armus, L., & Miley, G. K. 1987, Astronomical Journal (ISSN 0004-6256), 93, 276

—. 1990, Astrophysical Journal Supplement Series (ISSN 0067-0049), 74, 833

Heckman, T. M., et al. 2011, The Astrophysical Journal, 730, 5

Hopkins, P. F. 2012, Monthly Notices of the Royal Astronomical Society: Letters, 420, L8

Hopkins, P. F., Hernquist, L., Cox, T. J., Dutta, S. N., & Rothberg, B. 2008, The Astrophysical Journal, 679, 156

Hopkins, P. F., Hernquist, L., Cox, T. J., Matteo, T. D., Martini, P., Robertson, B., & Springel, V. 2005, The Astrophysical Journal, 630, 705

Hopkins, P. F., Keres, D., Murray, N., Quataert, E., & Hernquist, L. 2011, arXiv, astro-ph.CO

Kaufman, M., Bash, F. N., Kennicutt, R. C., & Hodge, P. W. 1987, Astrophysical Journal, 319, 61

Kennicutt, R. C. 1984, Astrophysical Journal, 287, 116

—. 1998, Astrophysical Journal v.498, 498, 541

Kewley, L. J., Groves, B., Kauffmann, G., & Heckman, T. 2006, Monthly Notices of the Royal Astronomical Society, 372, 961

Law, D. R., Steidel, C. C., Erb, D. K., Larkin, J. E., Pettini, M., Shapley, A. E., & Wright, S. A. 2009, The Astrophysical Journal, 697, 2057

Lehnert, M. D., & Heckman, T. M. 1995, Astrophysical Journal Supplement Series (ISSN 0067-0049), 97, 89

Leitherer, C., et al. 1999, The Astrophysical Journal Supplement Series, 123, 3

Martin, C. L. 2005, The Astrophysical Journal, 621, 227

—. 2006, The Astrophysical Journal, 647, 222
—. 2007, Galaxy Evolution Across the Hubble Time, 235, 280
Monreal-Ibero, A., Arribas, S., & Colina, L. 2006, The Astrophysical Journal, 637, 138
Murphy, T. W., Armus, L., Matthews, K., Soifer, B. T., Mazzarella, J. M., Shupe, D. L., Strauss, M. A., & Neugebauer, G. 1996, Astronomical Journal v.111, 111, 1025
Murray, N., Martin, C. L., Quataert, E., & Thompson, T. A. 2007, The Astrophysical Journal, 660, 211
Murray, N., Quataert, E., & Thompson, T. A. 2005, The Astrophysical Journal, 618, 569
Noguchi, M. 1999, The Astrophysical Journal, 514, 77
Osterbrock, D. E., & Ferland, G. J. 2006, Astrophysics of gaseous nebulae and active galactic nuclei
Overzier, R. A., et al. 2008, The Astrophysical Journal, 677, 37
—. 2009a, The Astrophysical Journal, 706, 203
—. 2009b, The Astrophysical Journal, 704, 548
—. 2011, The Astrophysical Journal Letters, 726, L7
Peterson, B. M. 2006, Physics of Active Galactic Nuclei at all Scales, 693, 77
Reyes, R., et al. 2008, The Astronomical Journal, 136, 2373
Rich, J. A., Kewley, L. J., & Dopita, M. A. 2011, The Astrophysical Journal, 734, 87
Rupke, D. S., & Veilleux, S. 2005, The Astrophysical Journal, 631, L37
Rupke, D. S., Veilleux, S., & Sanders, D. B. 2002, The Astrophysical Journal, 570, 588
—. 2005a, The Astrophysical Journal, 632, 751
—. 2005b, The Astrophysical Journal Supplement Series, 160, 87
—. 2005c, The Astrophysical Journal Supplement Series, 160, 115
Sanders, D. B., Scoville, N. Z., Young, J. S., Soifer, B. T., Schloerb, F. P., Rice, W. L., & Danielson, G. E. 1986, Astrophysical Journal, 305, L45
Schlegel, D. J., Finkbeiner, D. P., & Davis, M. 1998, Astrophysical Journal v.500, 500, 525
Schreiber, N. M. F., et al. 2006, The Astrophysical Journal, 645, 1062
Searle, L. 1971, Astrophysical Journal, 168, 327
Shapiro, K. L., et al. 2008, The Astrophysical Journal, 682, 231
—. 2009, The Astrophysical Journal, 701, 955
Shull, J. M., & McKee, C. F. 1979, Astrophysical Journal, 227, 131
Springel, V., Matteo, T. D., & Hernquist, L. 2005, Monthly Notices of the Royal Astronomical Society, 361, 776
Toomre, A., & Toomre, J. 1972, Astrophysical Journal, 178, 623
Veilleux, S., et al. 2009, The Astrophysical Journal Supplement, 182, 628
Weaver, R., Mccray, R., Castor, J., Shapiro, P., & Moore, R. 1977, Astrophysical Journal, 218, 377